



Lamb wave-based damage imaging of CFRP composite structures using autoencoder and delay-and-sum

Yinghong Yu, Xiao Liu, Yihan Wang, Yishou Wang, Xinlin Qing^{*}

School of Aerospace Engineering, Xiamen University, Xiamen, Fujian 361005, PR China



ARTICLE INFO

Keywords:

Ultrasonic guided wave
Composite structures
Delay-and-sum
Denoising autoencoder
Damage imaging

ABSTRACT

Ultrasonic guided wave is a promising technique for structural health monitoring and nondestructive testing. However, due to the anisotropy and complexity of composite materials, the imaging performance of numerous signal processing methods deteriorates with significant artifacts and unsatisfactory accuracy. To obtain a better damage imaging performance of Lamb waves in noisy and noise-free conditions, a weighted delay-and-sum (DAS) imaging method based on denoising autoencoder (DAE) learning is developed for complex composite structures. The traditional DAS formulation is modified to be more compatible with anisotropic materials. The DAE with feature learning capability is then employed to extract potentially efficient features and remove noise from ultrasonic signals. Several verification experiments conducted on flat or curved and stiffened composite structures have confirmed the ability of the DAE-DAS method to suppress artificial noise and to intensify singularities induced by the anomalies. By comparing with the unweighted DAS methods and the weighted DAS method without feature extraction, the proposed algorithm has satisfactory robustness to achieve higher localization accuracy and fewer artifacts.

1. Introduction

Composite materials are widely used in aerospace, atomic energy and electronics industries to reach higher specific strength, better fatigue/corrosion resistance performance and greater stiffness than traditional metallic materials. The extensive usage of composite materials increases the requirements for damage detection and integrity assessment of composite structures. Various damages such as crack, delamination, and matrix cracking may occur during the fabrication and in-service processes of composite materials, which will destroy the structural integrity of the composite and eventually lead to severe performance degradation and structural failure [1–3]. Structural health monitoring (SHM) systems have the capability to assess the potential failures and significantly improve the maintenance efficiency as well as reduce maintenance costs by converting scheduled maintenance to condition-based maintenance [4–6]. Consequently, SHM techniques for damage assessment and monitoring of composite materials have received considerable attention.

For SHM applications, the ultrasonic guided wave is a promising tool because of its large monitoring area with relatively low attenuation, sensitivity to diverse defects and high implementation efficiency [7]. In

a typical ultrasonic guided waves-based SHM system, piezoelectric lead zirconate titanate (PZT) sensors are commonly used to transmit and receive guided waves to assess the structural health status and realize damage detection [8]. As a critical part of damage detection, damage localization methods are able to visualize damage information and quickly locate anomalies, thus attracting many researchers. Therefore, various imaging technologies have sprung up, such as artificial neural network (ANN) [9,10], phased array imaging [11,12], sparse reconstruction (SR) [13,14], probability-based diagnostic imaging (PDI) [15–17] and delay-and-sum (DAS) [18–20] methods. A phased array is an array composed of multiple independent transducers to achieve precise phase and amplitude control of each element and to reconstruct the damage status of structures. However, it requires a relatively dense actuator-sensor network to improve the signal-to-noise ratio (SNR) level and to ensure the accuracy of damage location. Sparse reconstruction based on compressed sensing is an imaging method developed by Levine and Michaels in 2013 [21], which has received wide attention in the field of guided wave-based SHM. It effectively exploits the prior physical knowledge of response waves propagating in a plate-like structure under arbitrary excitation. The over-complete dictionary is constructed from the Lamb wave propagation model, and the damage imaging results can

* Corresponding author.

E-mail address: xinlinqing@xmu.edu.cn (X. Qing).

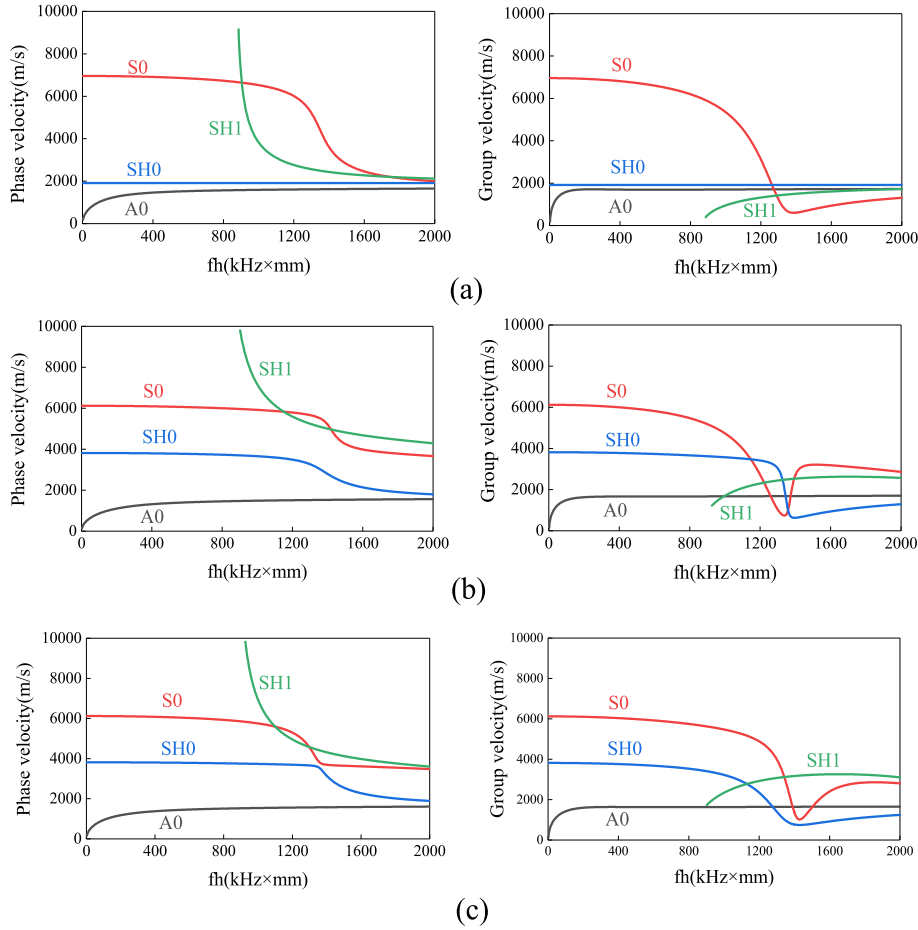


Fig. 1. Dispersion curves of Lamb waves traveling (a) along $\theta = 0^\circ$, (b) along $\theta = 30^\circ$, (c) along $\theta = 60^\circ$, where fh is the frequency multiplied by the plate thickness.

be directly obtained by solving the sparse coefficients problem with a convex optimization algorithm. Although the sparse reconstruction algorithm can achieve multi-damage detection, its imaging performance is limited in several aspects, such as high computational complexity, low detection efficiency and significant artifacts.

Delay and sum, belonging to sparse array imaging techniques, depends on a few sensors to locate anomalies. It is the most appealing imaging method due to its conceptual simplicity and easy implementation. This method was developed based on the synthetic time-reversal principle by Wang et al. in 2004 [22] for large-scale monitoring. Michaels et al. [23] extended the method to a DAS imaging method and successfully applied it to locate notched and simulated corrosion holes in aluminum plates. They also introduced an image fusion process to additionally reduce the intensity of artifacts. In addition, Michaels proposed a modified DAS algorithm based on windowed energy arrival and investigated the applicability of this algorithm for detecting barely visible impact damage (BVID) in isotropic and stiffened composite plates [24]. Their verification work demonstrated the feasibility of damage detection, but its damage localization accuracy was low for complex composite structures with multiple stiffeners. In addition, there are severe artifacts in the imaging results, which cause interference and degrade the imaging quality.

To counter application limitations, a guided wave-based imaging method for complicated structures is developed to predict damage localization by using a weighted delay-and-sum algorithm. The weighting factor is a damage sensitive index (DSI) calculated from the correlation between the baseline and current signals. However, conventional damage sensitive indices fail to extract useful features from the collected guided wave signals. Furthermore, the performance of all

imaging algorithms was tested in a noise-free experimental environment, but noise is unavoidable in industrial environments. Therefore, it is particularly important to extract stable and meaningful features from guided wave signals and denoise them to improve the damage location accuracy. ANN, as a powerful data-driven tool, can be combined with guided waves to successfully implement anomaly assessment of composite structures, including damage localization and quantification. Autoencoders, a commonly used artificial neural network, first emerged for dimensionality reduction and were later successfully used as denoising autoencoders, especially in the fields of automated medical imaging and speech recognition [25,26]. Therefore, a novel Lamb wave-based damage detection method is proposed for complex composite structures by integrating a denoising autoencoder (DAE) with a DAS algorithm, i.e., DAE-DAS. In this proposed method, the DAS algorithm is modified to be compatible with complex composite structures. Then, a denoising autoencoder is constructed to extract potential characteristics and reduce the noise from the original guided wave signals through hidden layers. In addition, an energy-based DSI is adopted to measure the difference between the measured signals and the baseline signals after auto-encoder feature extraction, which is weighted with the modified DAS algorithm for damage detection and location. The significant advantages of this method are the efficiency and accuracy in identifying damage information of complex composite structures in the presence or absence of noise environments, and the simplicity of operation without manual feature extraction. The superior performance of the proposed damage imaging method is demonstrated by practical experimental tests and some comparisons with other imaging methods.

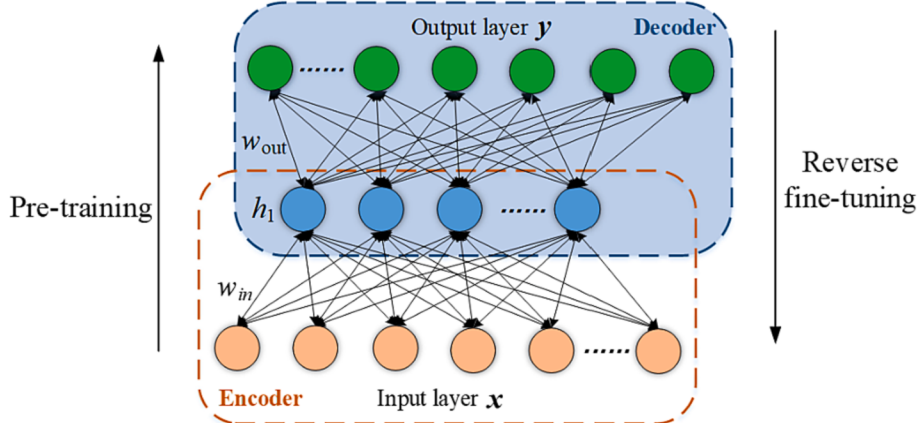


Fig. 2. The schematic diagram of the autoencoder structure.

2. Damage imaging based on the DAE-DAS method

In this section, the theoretical foundation of Lamb wave propagation in composite plate, the DAS method, autoencoder and the DAE-DAS method were presented.

2.1. Lamb wave signals

Lamb wave was first investigated by Horace Lamb in 1917 [27]. The guided elastic wave traveling in plate-like structures has three mode types: symmetric modes S_b , antisymmetric modes A_i and shear-horizontal SH_i , where i ($i=0, 1, \dots$) represents mode order. In composite materials, the phase velocity and group velocity are direction-dependent due to their inherent anisotropy and non-uniformity. A carbon fiber reinforced composite plastics (CFRP) plate with a layup of [0/90/0/90], was considered and the dispersion curves of waves propagating along with the directions 0°, 30° and 60° can be achieved by the free software LAMSS performed in MATLAB 2018b. It can be seen from Fig. 1 that Lamb waves traveling along different directions (0°, 30° and 60°) possess different phases and group velocities.

2.2. The weighted DAS imaging method

Most damage imaging algorithms detect changes induced by damage or service environments through the residual signals $R_{a,r}(t)$ of the baseline $B_{a,r}(t)$ and current signals $C_{a,r}(t)$. Hilbert transform, as a reliable method to efficiently calculate the amplitude envelope, is performed on the measured signals to compensate for the effect of phase differences. The envelope-detected residual signal $S_{a,r}$ for each pair of actuator sensor 'a' and receiver sensor 'r' is obtained from the Hilbert transform:

$$S_{a,r} = \text{abs}(\text{Hilbert}(R_{a,r})) \quad (1)$$

To operate the DAS imaging method, the time of flight (TOF) of a potential scattering source at position (x, y) is first calculated for all pairs of transmitters based on the knowledge of the group velocity. The value $E(x, y)$ of each location in the monitoring area is then obtained as follows [28]:

$$E(x, y) = \frac{1}{N(N-1)} \sum_{a=1}^{N-1} \sum_{r=a+1}^N S_{a,r}(t_{adr}(x, y)) \quad (2)$$

where N is the number of transducers and t_{adr} is the TOF of a wave transmitted from an actuator sensor 'a', received at point 'd' and then scattered back to receiver sensor 'r'. However, the conventional DAS method for damage detection assumes that the propagation velocity of the selected wave mode along all directions is a constant. This will lead to wrong detection results. In order to make Eq. (2) effective for

anisotropic composite structures, the group velocity is adjusted to $C_g = L_{a,r}/(T_b - T_{off})$, which is a frequency-dependent variable as it is related to the time of flight of the guided wave. For different signal excitation frequencies, the arrival time of the response signals is different, thus causing differences in the group velocity at different frequencies. $L_{a,r}$ is the distance between the transmitter and the receiver. Then, the TOF after correction can be calculated as follows [20]:

$$\hat{t}_{adr}(x, y) = \frac{L_{adr}}{C_g} + T_{off} = \frac{L_{adr}}{L_{a,r}} \cdot (T_b - T_{off}) + T_{off} \quad (3)$$

where T_{off} and T_b are the take-off time of the excitation signal and the arrival time of the baseline signal, respectively. L_{adr} is the sum of the distance from the location (x, y) to the actuator and the receiver. Since the signal gain and attenuation are various for different sensing paths, the DAS results need to be normalized according to the equation described below:

$$\widehat{E}_{a,r}(x, y) = \frac{E_{a,r}(x, y) \cdot L_{adr}(x, y)}{V_{a,r} G_{a,r}} = \frac{L_{adr}(x, y)}{V_{a,r} G_{a,r}} \cdot S_{a,r}(\hat{t}_{adr}(x, y)) \quad (4)$$

where $G_{a,r}$ and $V_{a,r}$ denote the signal gain and amplitude of the sensing path excited by the actuator sensor 'a' and received by the sensor 'r', respectively.

The modified DAS method can achieve higher accuracy as it contains properly useful information about guided waves. However, the measured signals may inevitably contain edge reflections and other interferences, especially in the corners and edges of the inspected plate. In order to achieve better imaging performance, a weighted DAS reconstruction model based on damage sensitive index is used to replace the construction model described in Eq. (4), such that.

$$P_{a,r}^{\text{new}}(x, y) = \sum_{a=1}^{N-1} \sum_{r=a+1}^N P_{a,r}^{\text{new}}(x, y) = \sum_{a=1}^{N-1} \sum_{r=a+1}^N DSI_{a,r}(x, y) \cdot \widehat{E}_{a,r}(x, y) \quad (5)$$

where $P_{a,r}^{\text{new}}(x, y)$ is the estimation probability of the sensing path excited by the actuator sensor 'a' and received by the sensor 'r' at location (x, y) . $DSI_{a,r}$ denotes the damage sensitive index. From Eq. (5), it can be seen that if the damage location is closer to the n -th sensing path, the DSI is larger and then a larger weight is placed on the n -th imaging matrix. Conversely, when the damage location is far from the n -th sensing path, the DSI will be smaller or even closer to zero, and then the weights on that sensing path will be smaller accordingly. Due to the unequal weights placed on the imaging matrix, the weighted DAS method reduces artifacts and improves the damage imaging performance. Since signal energy difference (SED) is an effective damage sensitive index, it is used in this study to weight with the modified DAS method and can be expressed as follows:

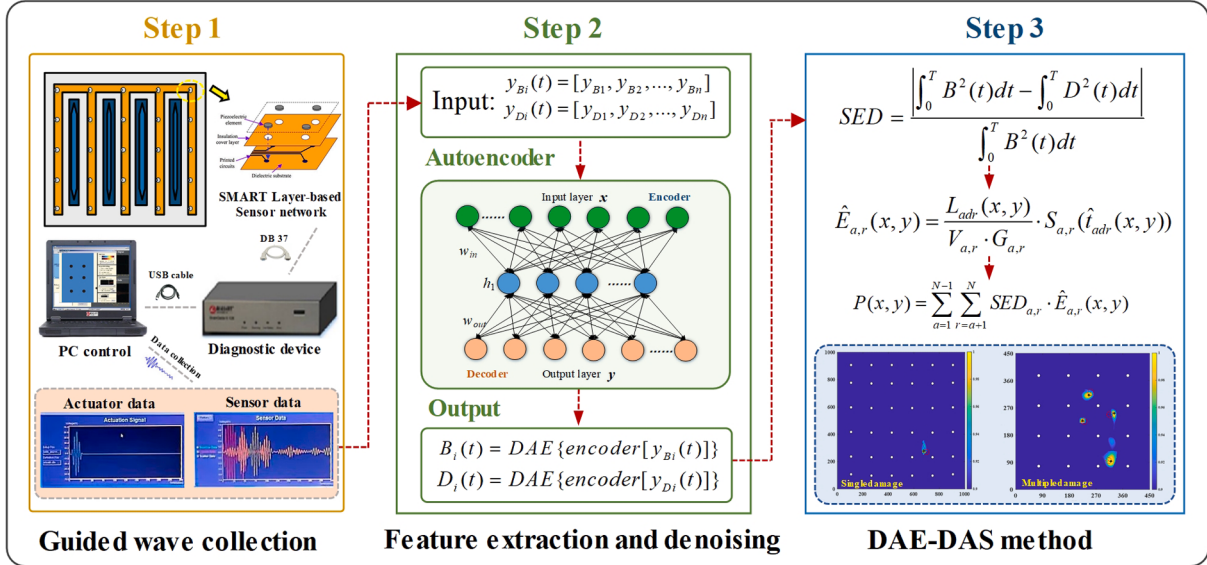


Fig. 3. The calculation process of the DAE-DAS imaging method.

$$SED = \frac{\left| \int_0^T B^2(t)dt - \int_0^T C^2(t)dt \right|}{\int_0^T B^2(t)dt} \quad (6)$$

where $B(t)$ and $C(t)$ are the pristine signal and the current signal, respectively. T is the time length of signal interception.

2.3. The proposed DAE-DAS imaging method

2.3.1. Autoencoders

To implement the proposed weighted DAS method, the first task is to extract the SED feature from the original guided wave signals. However, the length of the intercepted signal has a significant effect on the damage localization results, and it is difficult to extract damage features in noisy and feature-independent conditions. To improve the robustness of data features, an autoencoder is introduced to adaptively perform feature extraction and noise reduction of ultrasonic signals. Autoencoder is an artificial neural network that learns an effective representation of the

input data to complete the task of feature selection. It consists of two primary parts: encoder and decoder [29], as shown in Fig. 2. The encoder is the one that compresses the input data to the point of maximum compression and forces the neural network to learn useful and implicit features [30]. The point of maximum compression is called the feature space, and the decoder attempts to reconstruct the input with the data in the feature space. There are several types of autoencoder i.e., sparse autoencoder, denoising autoencoder and variational autoencoder. In denoising autoencoder, the model is forced to learn the reconstruction of noisy data given its non-noisy version. Suppose x_n is the noisy signal and x is the signal without noise. The encoder maps x_n to feature space and the decoder tries to reconstruct the non-noisy version of x_n from feature space. Eventually, mean square error (MSE) between decoder output and original input is calculated iteratively until it converges to a minimum value. This process can be represented by the following mathematical expression:

$$\text{Denoising} = \text{minimize} [\text{MSE}(\text{Decoder output}, \text{original input})] \quad (7)$$

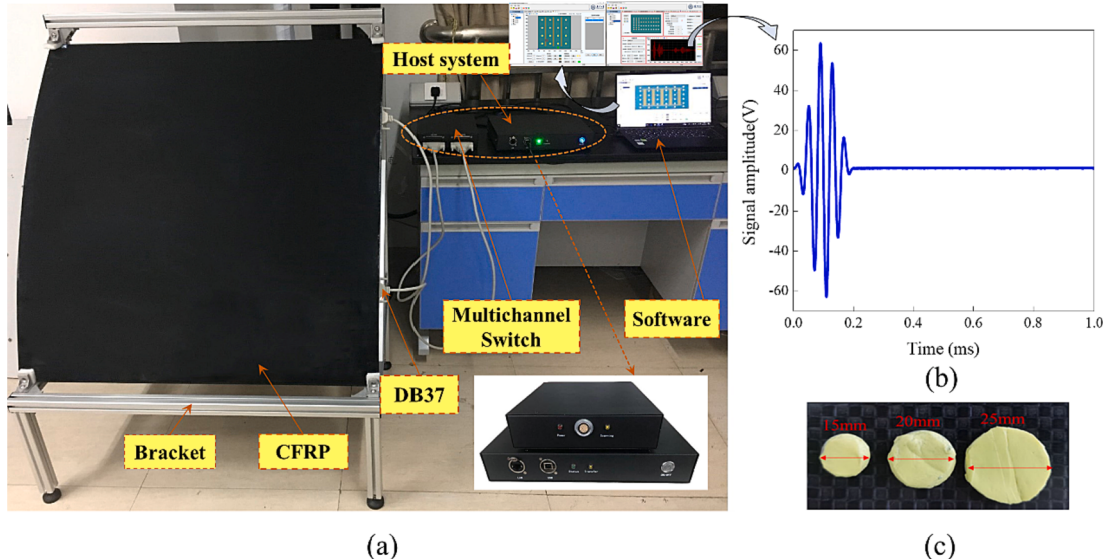


Fig. 4. The experimental setup for large-scale curved CFRP damage monitoring with guided wave. (a) Physical diagram of the specimen from front view. (b) The excited five-peak signal. (c) Photo of the artificial simulated defects.

Table 1

Technical indicators of the monitoring equipment used.

Technical parameters	Value
Conversion rates	48 MHz
Excitation frequency range	10 kHz ~ 1000 kHz
Output voltage range	Min: ± 10 V Max: ± 60 V
Memory	32,000 Samples
Sampling rates	6, 12, 24, 48 MHz/s
Resolution	12bit
ADC range	± 1 V
Gain adjustment range	10 dB–40 dB, step:1 dB

Table 2

Orthotropy properties of the CFRP with stiffeners [in GPa].

E_{11}	E_{22}	E_{33}	G_{12}	G_{13}	G_{23}	v_{12}	v_{13}	v_{23}
45.19	38.27	7.18	3.41	2.14	2.12	0.14	0.49	0.50
C_{11}	C_{12}	C_{13}	C_{22}	C_{23}	C_{33}	C_{44}	C_{55}	C_{66}
48.53	8.05	7.00	41.53	4.55	7.96	2.12	2.14	3.41

2.3.2. Autoencoder architecture

In this paper, a denoising autoencoder is employed for two main reasons. First, it is able to learn the reconstruction of the non-noisy version from the noise-added data. Second, it can compress the input data to the point of maximum compression and learn the effective representation of the input data. After collecting the guided wave signals from all sensing paths, the baseline and response signals are fed to the denoising autoencoder to learn the effective expression of the implicit features. The difference between the implicit features corresponding to the baseline data and the measured data is then calculated based on the SED and used as a weighting factor for the DAS algorithm. The first task of using the DAE algorithm is to determine optimal process parameters, but no uniform optimization rules have emerged. In this work, the cross-validation method is used to select the appropriate combination of parameters to maximize the advantage of the algorithm. The autoencoder used is designed in MATLAB 2018b. It has an input layer with nodes equal to the sampling points of the given signal i. e. 120000. Following the input layer, there is a hidden layer that forms an encoder with the input layer for compressing and extracting data features from the feature space. In this study, a hidden layer with 800 nodes is used to compress the input signal to 800 points. Proceeding to the feature space, there is an output layer that decodes the data in the feature space with the same

size as the input layer i. e. 120000. Then the MSE between the decoder output and the raw input data is computed until a user-defined maximum number of iterations is reached, which is set to 200 in this work. To better elucidate the methodology proposed, the generation principle of the imaging process is explained in a flowchart as demonstrated in Fig. 3.

3. Experiments and analysis

3.1. Experimental verification on a curved stiffened composite structure with simulated damages

3.1.1. Experimental setup

To verify the effectiveness of the proposed damage imaging method, an experimental platform based on guided wave monitoring was established for damage detection on a curved stiffened anisotropic composite aircraft siding. It consists of a monitoring system with a multichannel switch and host system, a software, and a bracket for CFRP, as shown in Fig. 4. The monitoring system developed by Dalian Junsheng Technology Co., allows supplying a five-cycle Hamming windowed sinusoidal waveform at the transmitter while obtaining measurements at the receiver. The main technical indicators are shown in Table 1. The stiffeners and the panel of the complex CFRP were manufactured by a liquid composite molding process (LCM) followed by co-cured together. The test resin used to impregnate the fibers is MERICAN® 30-200P with low viscosity and excellent properties in mechanical. The panel consists of T300 carbon fiber woven cloth in a stacking configuration of $[#(0/90)]_{15}$ with dimensions of 1000 mm × 1000 mm × 3 mm and a radius of curvature of 2000 mm. The relevant properties are shown in Table 2 and the fiber density is 1780 kg/m³. The longitudinal stiffeners have dimensions of 640 mm × 50 mm × 6 mm and a distance of 160 mm from the boundary, while the transverse stiffeners have dimensions of 740 mm × 30 mm × 3 mm and a distance of 150 mm from the boundary. To facilitate the composite aircraft siding to obtain the desired damage, absorbing materials were attached to different locations of the exterior siding to simulate artificial damage, which is a solid adhesive tape (provided by Easy Composites) with diameters of 15 mm, 18 mm, 20 mm, 25 mm and 30 mm, as partially shown in Fig. 4(c). The inherent stickiness of this solid tape easily drives it to adhere to the surface of the material and induce simulated damages with different sizes.

The Lamb wave propagating in the composite aircraft siding is complicated due to excessive attenuation and the presence of stiffeners.

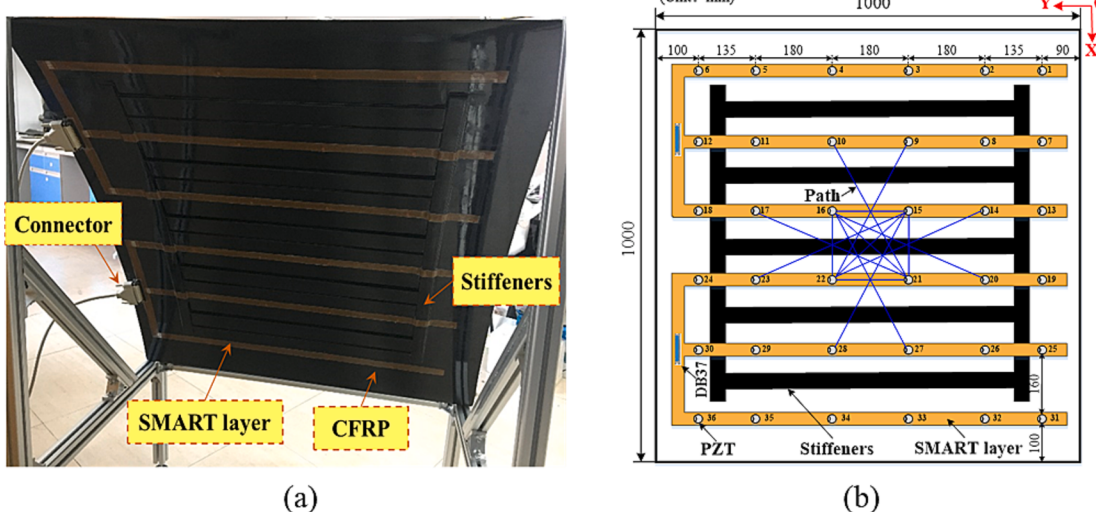


Fig. 5. The sensor layout and representative sensing paths of the large-scale curved CFRP plate. (a) Physical diagram of the specimen from back view. (b) Diagrammatic sketch of the sensors.

Table 3

The representative sensing paths and the excitation characteristics of the piezoelectric sensor network.

Path	Frequency (kHz)	Gain(dB)	Amplitude (V)	Path	Frequency (kHz)	Gain(dB)	Amplitude (V)
P16_15	35	30	55	P15_28	30	35	60
P16_20	40	40	60	P14_22	45	40	60
P16_21	35	30	60	P21_10	25	40	60
P16_22	35	30	55	P21_22	40	30	55
P15_21	45	30	55	P9_22	25	40	60
P15_22	25	30	60	P17_21	50	40	60
P15_23	30	40	60	P27_16	30	35	60

(Note: P16_15 represents PZT 16 excitation and PZT 15 reception).

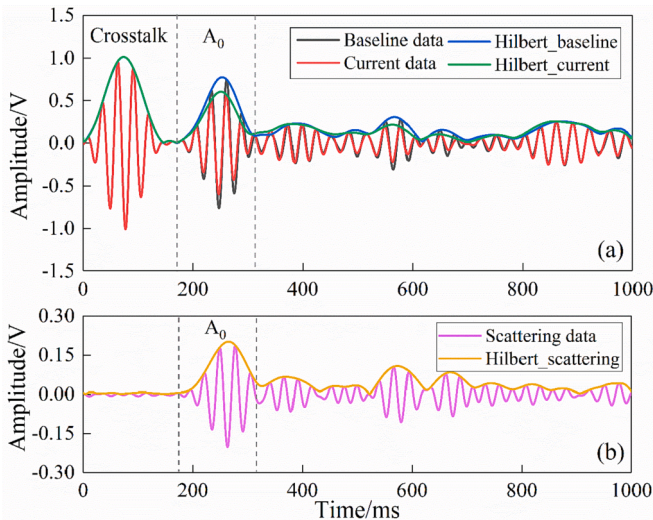


Fig. 6. An example of the collected guided wave data. (a) The baseline data and current data, and their Hilbert transform results. (b) The scattering data and Hilbert transform result.

In order to effectively generate and detect Lamb wave, six identical Stanford Multi-Actuator-Receiver Transduction Layers (SMART) [31,32] with a total of thirty-six PZT sensors were firmly adhered to the surface of the structure using an epoxy adhesive (Hysol EA 9394). The adhesive can be cured at room temperature and has a high bonding strength. The SMART Layer is a network of piezoelectric elements supported on a thin flexible printed circuit substrate. The polyimide film used as a flexible substrate has excellent temperature resistance and can

operate at temperatures above 176 °C (350 °F). In addition, the flexibility allows it to bond well to the curved surface, as shown in Fig. 5. The PZTs used to generate Lamb wave in the experiment are circular PZTs with 8 mm diameter and 0.33 mm thickness. Since the structure with stiffeners is so complex that affects the propagation properties of the guided wave, 190 acquisition paths were set to completely cover the host structure with the guided wave signals and improve the damage detection-location precision and imaging resolution. Due to the differences in the local structural properties of CFRP, the performance of the piezoelectric sensors and the thickness of the adhesion layer during sensor adhesion, different parameter settings for different sensing paths should be specified. Based on the two main principles of easy mode classification and sensitivity to defects, the optimal excitation frequency, gain and amplitude for each sensing path were obtained by the parameter scanning method. The representative sensing paths and the excitation characteristics of the piezoelectric sensor network are shown in Table 3. Considering that the A₀ mode is more sensitive to scattering from surfaces (such as surface stickers), it is the preferred choice for damage detection in guided waves-based SHM systems [33].

3.1.2. Performance assessment of the weighted DAS method

Fig. 6 shows the guided wave signals, including baseline data, current data and scattering data, along with their Hilbert results when the virtual damage with a diameter of 20 mm is located at (443 mm, 585 mm). Then, the TOF characteristics of the baseline data T_b and current data T_c can be obtained.

Fig. 7 and Fig. 8 show the damage reconstructed results based on the weighted DAS algorithm and the unweighted DAS algorithm with a 90 % image threshold to minimize extraneous background noise and to highlight damage locations without excessive distortion. In this paper, the unweighted DAS algorithm contains both the modified DAS algorithm and the conventional DAS algorithm. As shown in these figures, the weighted DAS algorithm displays superior prediction performance

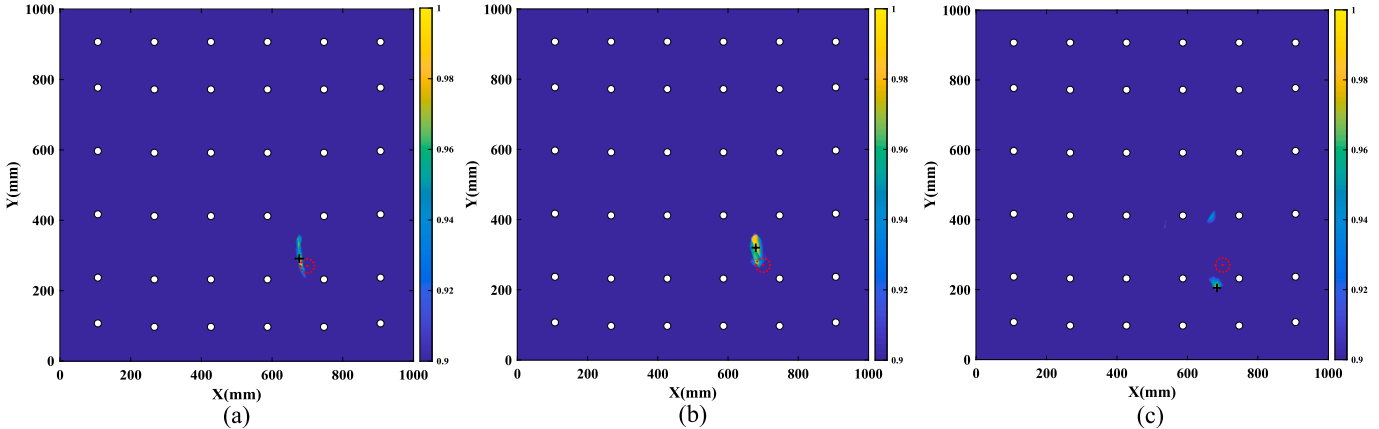


Fig. 7. The image reconstructed results of the complex CFRP plate via (a) the weighted DAS method, (b) the modified DAS method and (c) the conventional DAS method when the 15 mm diameter damage is located at (700 mm, 270 mm). White circles denote the PZTs, the center of the red dotted circle represents the actual location of damage and the black plus denotes the predicted damage location. (The meaning of these presented marks herein applied to all the following imaging results). (For interpretation of the references to colour in this figure legend, the reader is referred to the web version of this article.)

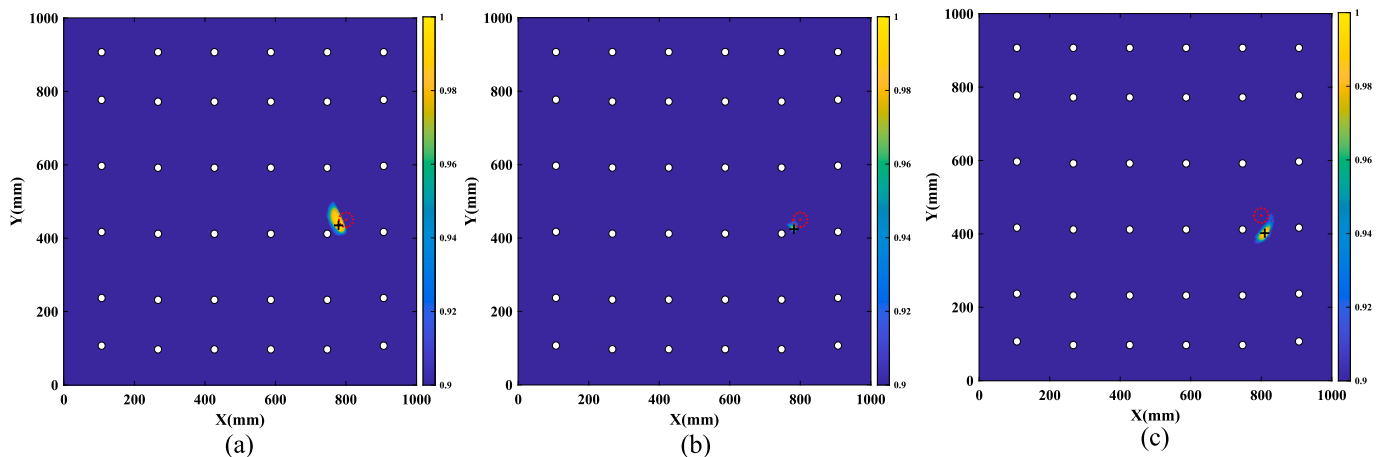


Fig. 8. The image reconstructed results of the complex CFRP plate via (a) the weighted DAS method, (b) the modified DAS method and (c) the conventional DAS method when the 25 mm diameter damage is located at (800 mm, 450 mm).

Table 4
Comparison of localization accuracy between different damage imaging algorithms.

Damage size	Damage center	DAE-DAS	RDE/mm	weighted DAS	RDE/mm	Modified DAS	RDE/mm	Conventional DAS	RDE/mm
D01_15	(700,270)	(680,277)	21.19	(676,287)	29.41	(680,320)	53.85	(684,205)	66.94
D02_25	(800,450)	(792,444)	10.00	(779,435)	25.81	(782,424)	31.62	(810,402)	49.03
D03_15	(146,195)	(154,193)	8.246	(160,174)	25.24	(184,161)	50.99	(238,198)	92.05
D04_25	(420,585)	(419,580)	5.099	(419,580)	5.099	(427,581)	8.062	(403,578)	18.38
D05_20	(502,490)	(500,506)	16.12	(497,462)	28.44	(507,458)	32.39	(524,409)	83.93
D06_18	(260,900)	(263,895)	5.831	(259,897)	3.162	(264,896)	5.657	(255,925)	25.49
D07_15	(302,400)	(304,398)	2.828	(305,405)	5.831	(303,410)	10.05	(320,390)	20.59
D08_30	(420,405)	(417,407)	3.606	(417,402)	4.243	(424,412)	8.062	(404,392)	20.62
D09_20	(485,585)	(470,584)	15.03	(476,571)	16.64	(462,595)	25.08	(480,626)	41.30
D10_18	(660,670)	(665,667)	5.831	(668,667)	8.544	(659,648)	22.02	(651,551)	119.3
Average			9.378		15.24		24.78		53.76

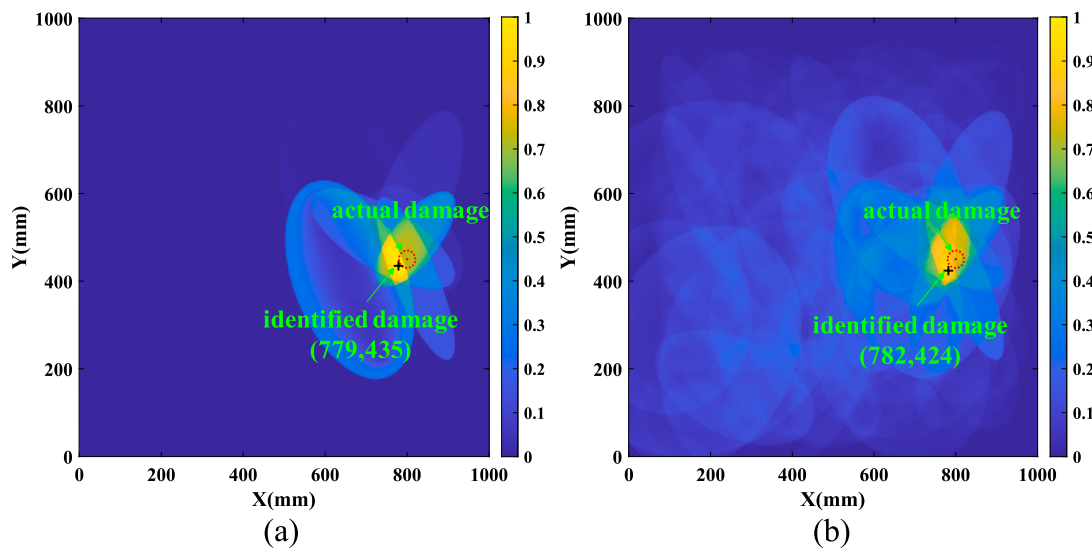


Fig. 9. The original image reconstructed results for damage-2 at coordinates (800 mm, 450 mm) via (a) the weighted DAS method and (b) the modified DAS method.

for different locations and different sizes of damage (damage-1: the 15 mm diameter damage located at (700 mm, 270 mm); damage-2: the 25 mm diameter damage located at (800 mm, 450 mm)) compared with the unweighted DAS methods. The results of the two damage localizations based on the three methods are enumerated in [Table 4](#). The relative distance error (RDE) is the Euclidean distance between the actual damage center and the identified location, and is a good statistic to measure the performance of the imaging method. It is worth noting that

artificial damage is intentionally attached to the intersection of two paths in order to make it easier to identify, but it is still difficult for the conventional DAS algorithm to locate the damage location due to the presence of the stiffener. Compared with the conventional DAS method, the RDE of the modified DAS method is reduced by 19.55 % for damage-1 and 35.51 % for damage-2. Although the modified DAS method gives better prediction accuracy, its accuracy still requires further improvement. The application of the weighted coefficient SED gives a powerful

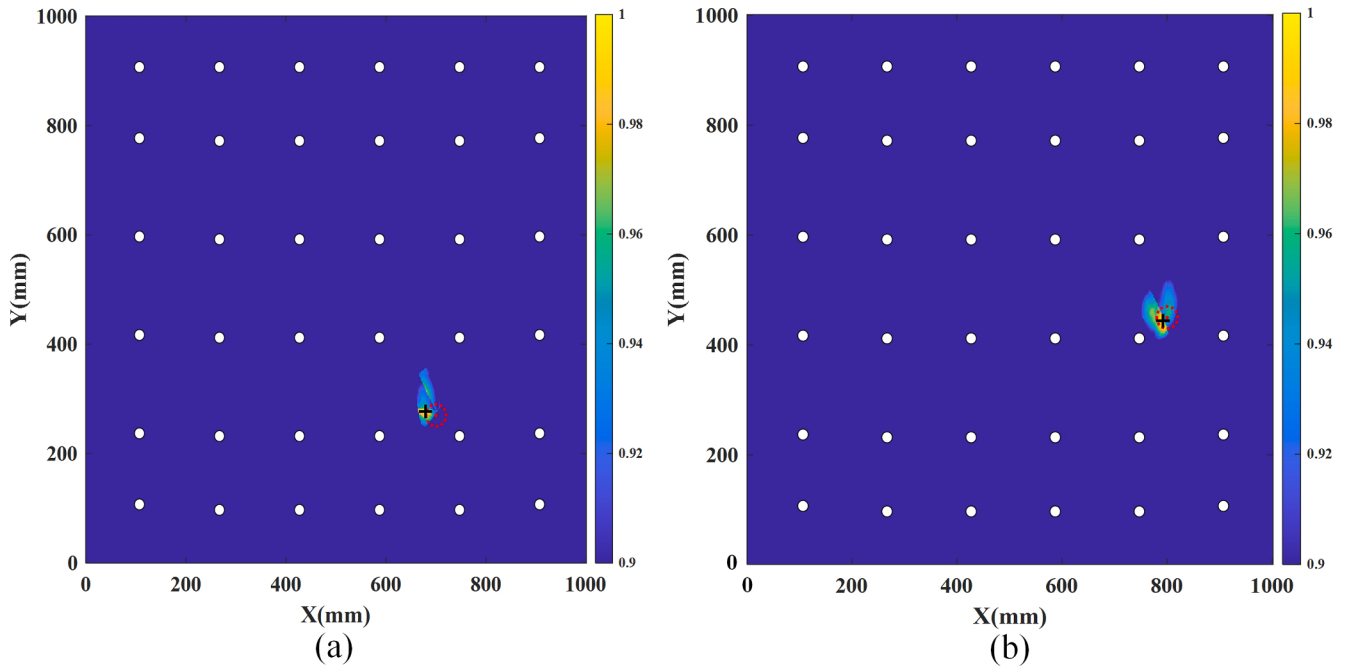


Fig. 10. The image reconstructed results of damage-1 at (a) (700 mm, 270 mm) and damage-2 at (b) (800 mm, 450 mm) on the complex CFRP plate via the DAE-DAS method.

fine-tuning capability and the final damage position precision is efficiently improved. For damage-1 shown in Fig. 7, the RDE of the weighted method is 45.38 % and 56.06 % lower than that of the modified and the conventional DAS methods, while 18.37 % and 47.36 % lower for damage-2. The imaging with SED weighting increases the pixel values close to the damaged area and decreases it far from the damaged location, and most of the damage-independent background noise was successfully eliminated. This phenomenon helps to reduce most of the artifacts that appear in the conventional reconstructed images, improves the SNR level and makes the imaging results more intuitive, as shown in Fig. 9. However, when exposed to the actual usage environment, the structure is susceptible to external noise, which will significantly weaken the damage assessment capability of the weighted DAS. To address this issue, an autoencoder with denoising capability is introduced in this paper to further improve the applicability of the weighted DAS method.

3.1.3. Feature extraction and denoising evaluation of the DAE-DAS method

The imaging results of damage-1 and damage-2 based on the DAE-DAS reconstruction method are displayed in Fig. 10. The damage prediction performance of the weighted DAS and DAE-DAS methods can be further compared by the imaging results of Fig. 10 (a) and Fig. 7(a) as well as Fig. 10 (b) and Fig. 8(a). It can be clearly seen that the prediction results of the DAE-DAS method shown in Fig. 10 (a) are closer to the actual damage location than the weighted DAS method shown in Fig. 7 (a). For damage-1 with coordinates (700 mm, 270 mm), the predicted coordinates of the DAE-DAS and the weighted DAS methods are (680 mm, 277 mm) and (676 mm, 287 mm) respectively, as shown in Table 4. The RDE of the DAE-DAS method is 27.95 % lower than that of the weighted DAS method while is 61.26 % lower for damage-2 with coordinates of (800 mm, 450 mm), indicating the effectiveness of the proposed method for feature extraction.

In addition, Table 4 presents several cases of identifying different damage sizes and locations based on four imaging methods (DAE-DAS, weighted DAS, modified DAS and conventional DAS methods). By comparing the predicted results of the four methods, a quantification of the damage localization accuracy can be obtained. The DAE-DAS method more accurately reflects the effect of the damage state on the

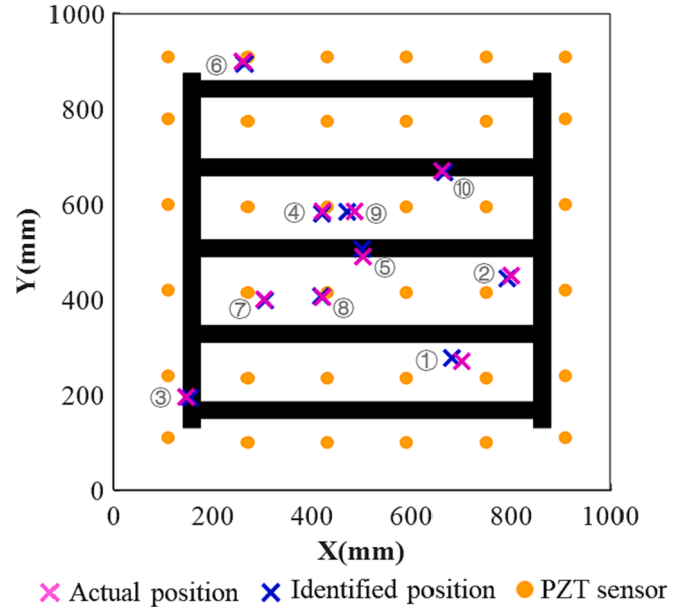


Fig. 11. Schematic diagram of ten simulated damage locations.

received signals and yields accurate localization results, achieving a minimum RDE prediction error of 9.378 mm. Although the modified DAS contributes to improving the damage localization accuracy compared to the conventional DAS, the DAE-DAS method achieves a much higher SNR level and more accurate anomaly location compared with the modified DAS method. For simulated damage at coordinates (146 mm, 195 mm) and (502 mm, 490 mm), the accuracy of the proposed method is 42.86 % and 90.48 % higher in X-direction, and 60 % and 42.86 % higher in Y-direction than that using weighted DAS methods. By comparing the damage location results of the four methods, the effectiveness of feature extraction of the presented methodology can be convincingly proved once more. In addition, Fig. 11 shows the imaging results of damage at different locations based on the proposed

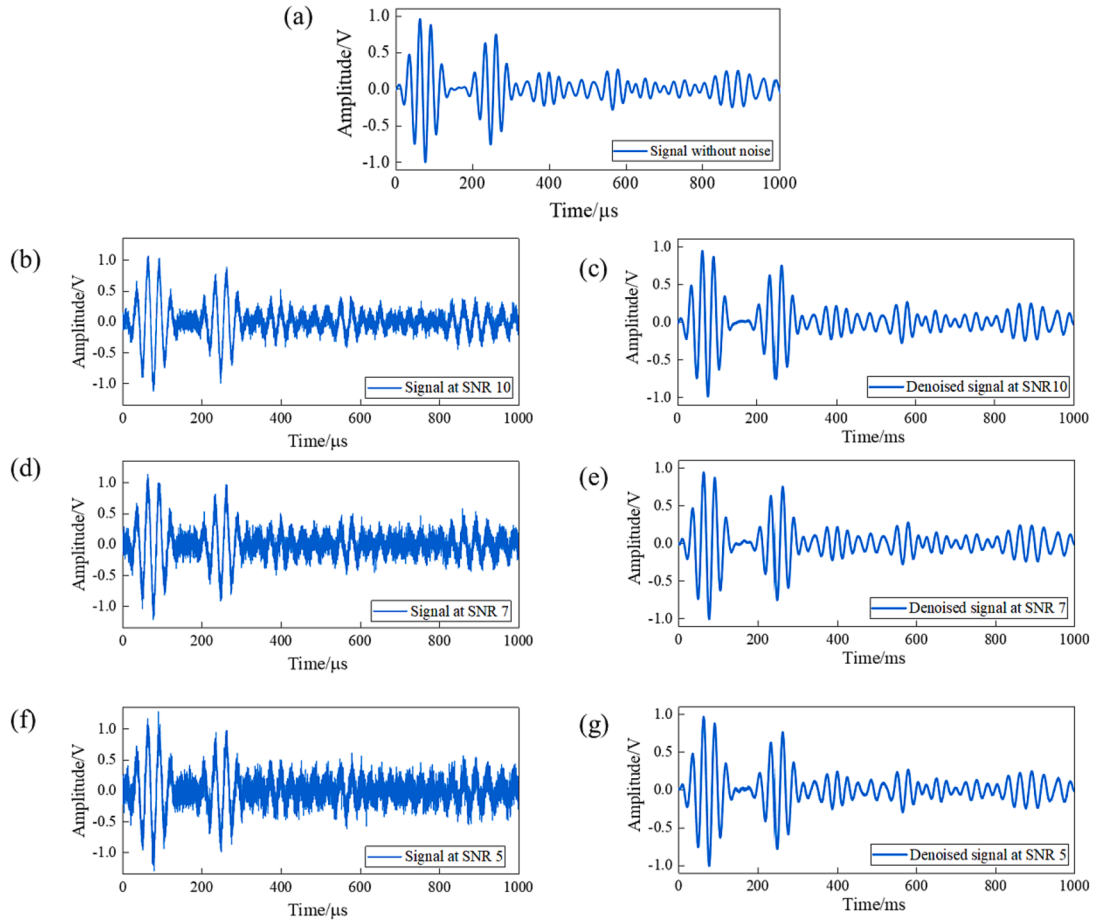


Fig. 12. Denoised guided wave signals by autoencoder. (a) Signal without noise; (b) Signal at SNR 10; (c) Denoised signal at SNR 10; (d) Signal at SNR 7; (e) Denoised signal at SNR 7; (f) Signal at SNR 5; (g) Denoised signal at SNR 5.

algorithm. It can be seen from the Fig. 11 that the damage identification location is consistent with the actual damage location, further proving the effectiveness of the DAE-DAS method.

Furthermore, additive white Gaussian noise (AWGN) is used to represent the electronic noise in the ultrasonic systems to further validate the denoising ability and robustness of the proposed algorithm. The complete description and mathematical details of AWGN are presented in Ref. [29]. Three different SNR levels i.e., SNR 5 (highest noise), SNR 7 and SNR 10 (lowest noise) of noise were added to the original guided wave signals. In this fashion, four different versions of each guided wave signal are developed, i.e., data without noise and data with SNR 5, SNR 7 and SNR10. The next step after adding noise was to evaluate the denoising performance of the autoencoder. The guided wave signals at SNR 5, SNR 7 and SNR 10 are combined to train the autoencoder against the signals without noise. It can be seen from Fig. 12 that the autoencoder successfully removed the noise from the contaminated data. The reconstructed MSE for the signals at SNR 5 was largest with value 1.252×10^{-4} , while was 6.514×10^{-5} and 6.422×10^{-5} for SNR 7 and SNR 10 respectively. It should be emphasized that the DAE is used not only for noise reduction but also for feature extraction to further improve the localization accuracy. Although several methods (such as bandpass filter, digital filter and wavelets) may achieve a noise reduction accuracy approaching the DAE method, they can only achieve the same localization accuracy as the weighted DAS to the maximum extent due to the lack of feature extraction capability.

Signals with the same AWGN of three different SNR levels were employed to evaluate the performance of the four damage imaging methods, and the comparison results for SNR 10 were displayed in Fig. 13. An absorbing wave material with a radius of 15 mm was

attached to the surface of the anisotropic composite structure at (800 mm, 450 mm) to induce damage. It can be seen from Fig. 13 that the DAE-DAS method provides reconstructed imaging results that accurately show the current damage state and the maximum peak value is consistent with the actual damage location because it achieves the maximum noise reduction. However, the other three DAS methods have severe artifacts and fail to indicate the correct damage location due to the lack of denoising capability. The DAE-DAS method gave 92.66 % better accuracy than the weighted DAS method, while gave 92.62 % and 92.77 % better than the modified DAS and conventional DAS methods. The quantitate-based outcomes demonstrated that the proposed imaging algorithm combining DAE and modified DAS can identify the damage location of the large-scale curved CFRP plate with significantly higher accuracy, demonstrating the effectiveness of the DAE-DAS in noise reduction and feature extraction.

3.2. Experimental verification on actual through-hole damage

3.2.1. Experimental setup

To further validate the method mentioned in section 2.3, actual through-hole damage was performed on a plate-like structure instead of simulated damage, as shown in Fig. 14. A multifunction hand drill (modal MNT 070610) developed by DEGUQMNT is employed to complete the drilling operation. The simple composite plate consists of six layers of T700 12 K carbon fiber preps in a stacking configuration of [0/90/0/90/0/90] with dimensions of 450 mm × 450 mm × 3 mm. They were cured at a constant temperature of 105°C for 3 h. Table 5 shows the mechanical properties of the unidirectional T700 prepreg, where the independent elastic constants of the stiffness matrix can be

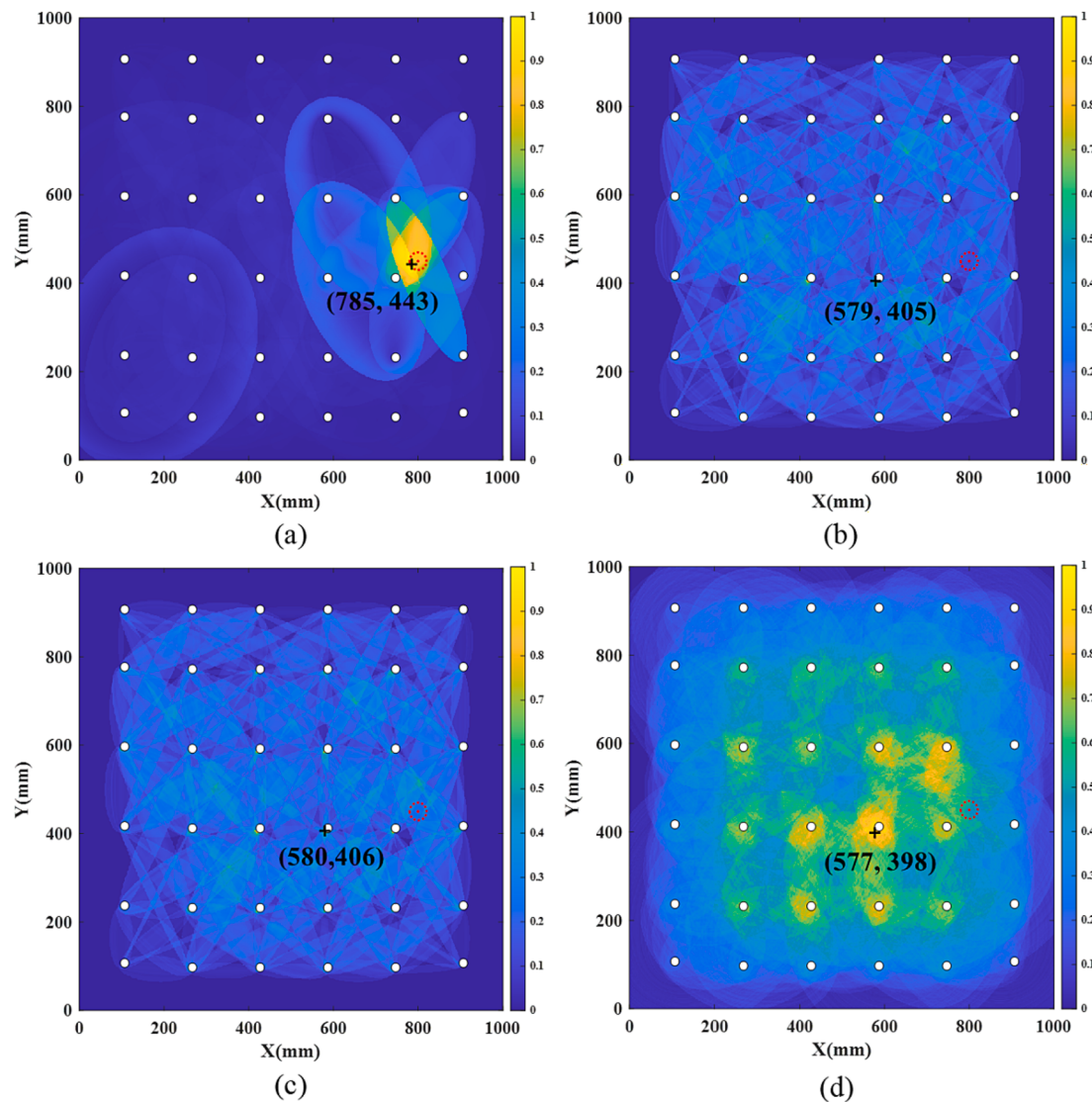


Fig. 13. The image reconstructed results of damage-1 on the complex CFRP plate via (a) the DAE-DAS, (b) the weighted DAS, (c) the modified DAS and (d) the conventional DAS methods.

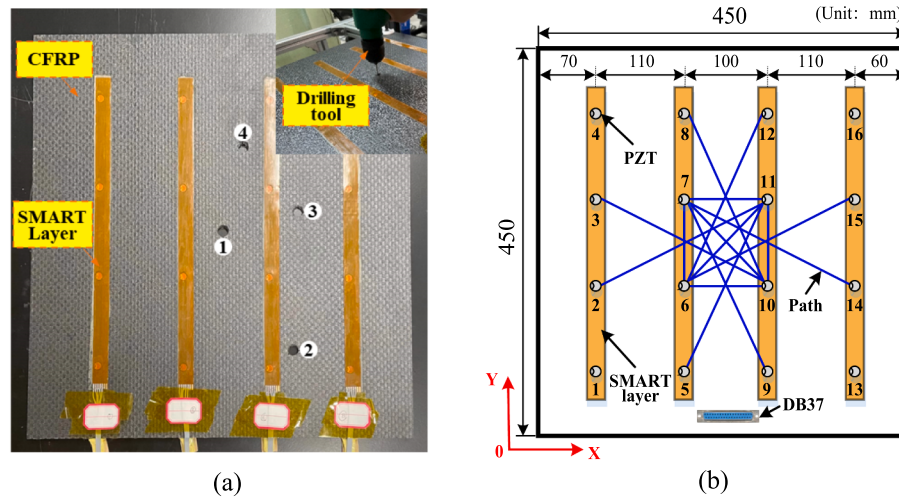


Fig. 14. (a) The CFRP plate with four actual through-hole damage. (b) The sensor layout and representative sensing paths.

Table 5
Material constants of T700 prepreg.

C_{11}	C_{12}	C_{22}	C_{23}	C_{66}	ρ
130 GPa	6.06 GPa	11.2 GPa	5.19 GPa	4.14 GPa	1571 kg/m ³

reduced to five by the assumption of transverse isotropy. The effect of damage at different locations with a diameter of 12 mm on the predicted results was experimentally investigated. Fig. 14(b) shows fourteen representative sensing paths marked by solid blue lines.

3.2.2. Performance comparisons

Subsequently, the drilling-induced multiple damage on the CFRP plate was investigated on the basis of experimental data to sufficiently demonstrate the effectiveness of the proposed methodology. There are six sensing paths for monitoring each subregion, including two diagonal and four edge channels. Fig. 15 demonstrated the time-domain response signals of the guided waves when the four through-holes of 12 mm diameter are located at different positions on the CFRP plate. Since it is difficult to obtain the interaction between signal variation and the damage location, the subareas monitoring technique proposed by Qiu [6] was introduced to further extend the application of the proposed method and to predict the location of the porous damage, as shown in the schematic diagram of Fig. 16. The basic principle of the subarea monitoring technique is to calculate the mean DSIs (MDSI) of each sub-area and to execute the proposed method for the subareas where the MDSI exceeds a preset threshold until the detection and localization of the entire structural damage is achieved.

Fig. 17 shows the reconstructed images of the four-hole damage obtained by the four approaches. The current guided wave signal covers the location information of the four holes and the imaging quality would deteriorate when multiple damages occur simultaneously. It can be seen that the conventional DAS result depicted in Fig. 17(d) demonstrated a relatively significant error. The four damage location results of the four methods were enumerated in Table 6, respectively. For multi-damage localization, both the conventional and modified DAS methods fail to locate all hole damage with high accuracy, but the newly developed method can yield accurate results with an RDE within 9.993 mm. Furthermore, it can be clearly seen that the proposed method can significantly improve the damage localization performance and suppress the noise level of the imaging results to highlight the damage information compared with the conventional DAS and modified DAS methods. It is not easy to identify multiple damages in different regions of the composite plate using only one set of guided wave signals. The fabrication quality of the hole damage also directly affects the guided wave signals during the practical operation of the experiment. As a result, the prediction errors between multiple damages may yield large differences when identified simultaneously.

In this work, CFRP laminates with and without stiffeners are used as an example and high-accuracy damage assessment results are obtained in a strong noise environment based on the proposed method, whereas the fundamental research idea can be extended to other SHM applications with excessive environmental variations. However, in damage assessment under high temperature or overload conditions, more complex dispersion and mode coupling effects will make signal interpretation problematic. Future work will attempt to extract guided-wave

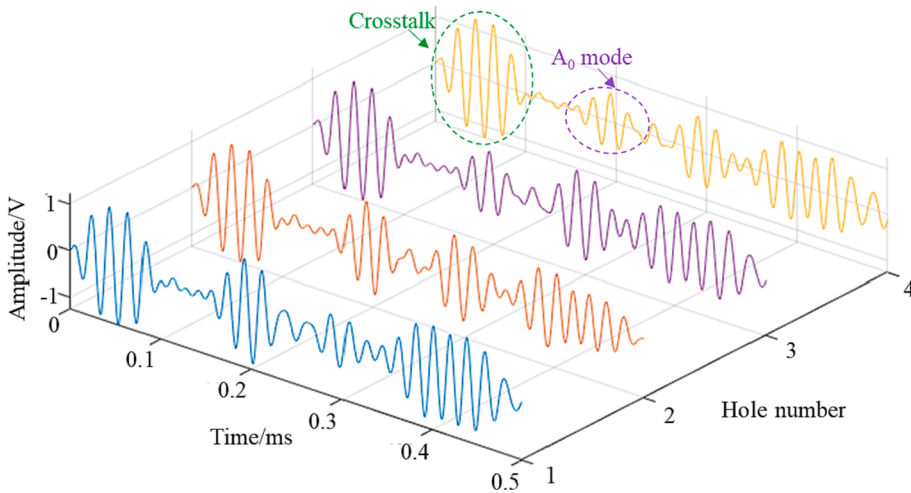


Fig. 15. Response signals of guided waves with the increasing number of holes.

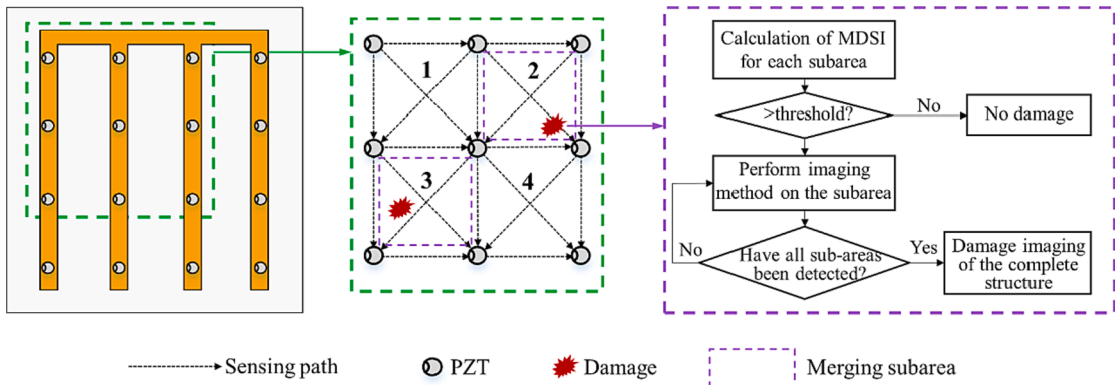


Fig. 16. The diagrammatic sketch of multi-damage localization.

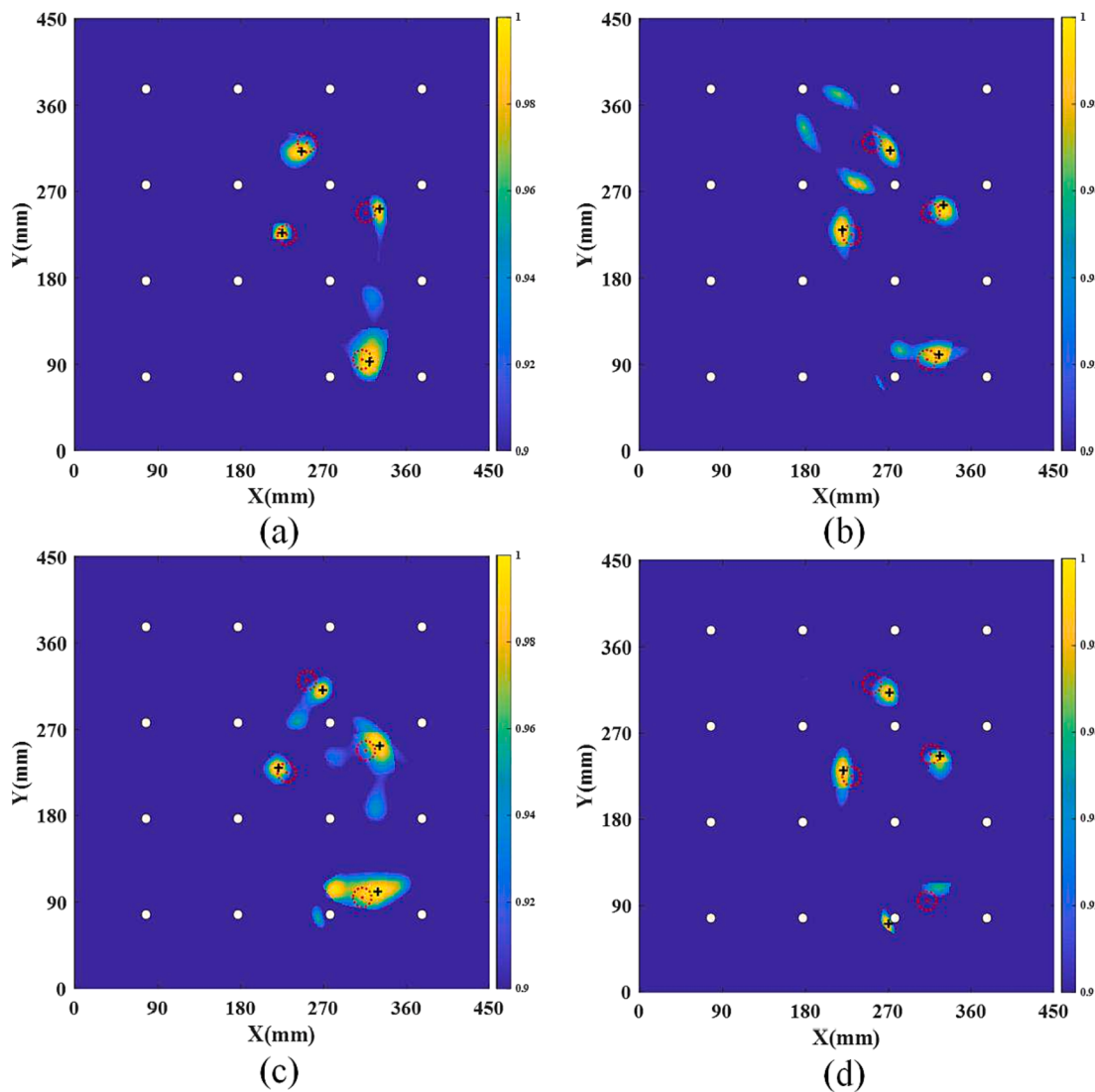


Fig. 17. Image reconstructed of porous damage via (a) the DAE-DAS, (b) the weighted DAS, (c) the modified DAS and (d) the conventional DAS methods.

Table 6

Comparison of localization accuracy between different damage imaging algorithms.

	Damage center	DAE-DAS	RDE/mm	Weighted DAS	RDE/mm	Modified DAS	RDE/mm	Conventional DAS	RDE/mm
D01	(230,225)	(225,227)	5.385	(220,230)	11.18	(221,230)	10.29	(221,231)	10.82
D02	(312,95)	(320,93)	8.246	(325,100)	13.93	(329,101)	18.03	(270,71)	48.37
D03	(316,248)	(331,252)	15.52	(330,256)	16.12	(331,253)	15.82	(326,246)	10.20
D04	(252,321)	(246,312)	10.82	(272,313)	21.54	(269,311)	19.72	(271,312)	21.02
Average		9.993			15.69		15.97		22.60

(Unit:mm).

characteristics independent of excessive environmental conditions (e.g., high temperatures or overloads) using the developed methods to eliminate the effects on the guided-wave signal, achieving in-situ and real-time SHM of composite structures. In addition, although the proposed method DAE-DAS achieves satisfactory localization accuracy, parameter optimization and time-consuming training process are also issues that need to be addressed in future work.

4. Conclusions

In this study, a novel damage imaging methodology combining an autoencoder and modified DAS is proposed to improve the performance of damage localization on complicated composite structures under noisy

and noiseless conditions. Two achievements were made in the conventional DAS imaging method. Firstly, the conventional DAS method is adjusted to apply to the damage assessment of anisotropic composite materials, and then the weighted factor SED is weighted with the modified DAS algorithm to improve the damage location capability. Another positive point of the weighted DAS method is its capability to suppress noise and improve image quality quite well under noise-free conditions. However, its performance degraded rapidly in high-noise environments. Therefore, a denoising autoencoder is applied to extract potentially useful features and reduce noise from the guided wave signals. The performance of the DAE-DAS imaging method is validated by some experiments conducted on the stiffened curved composite structure with simulated damage and a plate-like structure with multiple

through-hole damage. The reconstructed images demonstrate that the damage identification capability of the DAE-DAS approach is substantially better than that of the weighted DAS, modified DAS, and conventional DAS methods both in the laboratory environment and in the strong noise condition.

CRediT authorship contribution statement

Yinghong Yu: Conceptualization, Data curation, Methodology, Formal analysis, Writing – original draft. **Xiao Liu:** Visualization, Investigation. **Yihan Wang:** Formal analysis, Methodology, Validation. **Yishou Wang:** Supervision, Writing – review & editing. **Xinlin Qing:** Conceptualization, Supervision, Methodology, Funding acquisition, Resources, Writing – review & editing.

Declaration of Competing Interest

The authors declare that they have no known competing financial interests or personal relationships that could have appeared to influence the work reported in this paper.

Data availability

The authors do not have permission to share data.

Acknowledgments

This work was supported by National Natural Science Foundation of China (under Grant Nos. U2141245 and 11972314) and China Scholarship Council. The authors would also like to acknowledge COMAC Shanghai Aircraft Design and Research and CRRC Qingdao Sifang Co., Ltd. for the CFRP samples provided.

References

- [1] Zhu J, Wang Y, Qing X. A real-time electromechanical impedance-based active monitoring for composite patch bonded repair structure. *Compos Struct* 2019;212: 513–23.
- [2] Li J, Yu Y, Qing X. Embedded FBG sensor based impact identification of CFRP using ensemble learning. *Sensors* 2021;21(4):1452.
- [3] Qing X, Li W, Wang Y, Sun H. Piezoelectric transducer-based structural health monitoring for aircraft applications. *Sensors (Basel)* 2019;19:1–27.
- [4] Zhu J, Qing X, Liu X, Wang Y. Electromechanical impedance-based damage localization with novel signatures extraction methodology and modified probability-weighted algorithm. *Mech Syst Sig Process* 2021;146:107001.
- [5] Miorelli R, Fisher C, Kulakovskiy A, Chapuis B, Mesnil O, D’Almeida O. Defect sizing in guided wave imaging structural health monitoring using convolutional neural networks. *NDT and E Int* 2021;122:102480.
- [6] Qiu L, Liu M, Qing X, Yuan S. A quantitative multidamage monitoring method for large-scale complex composite. *Struct Health Monit: Int J* 2013;12(3):183–96.
- [7] Ren Y, Qiu L, Yuan S, Fang F. Gaussian mixture model and delay-and-sum based 4D imaging of damage in aircraft composite structures under time-varying conditions. *Mech Syst Sig Process* 2020;135:106390.
- [8] Wu J, Xu X, Liu C, Deng C, Shao X. Lamb wave-based damage detection of composite structures using deep convolutional neural network and continuous wavelet transform. *Compos Struct* 2021;276:114590.
- [9] Zhang S, Li CM, Ye W. Damage localization in plate-like structures using time-varying feature and one-dimensional convolutional neural network. *Mech Syst Sig Process* 2021;147:107107.
- [10] Qing X, Liao Y, Wang Y, Chen B, Zhang F, Wang Y. Machine learning based quantitative damage monitoring of composite structure. *Int J Smart Nano Mater* 2022;13(2):167–202.
- [11] Yu L, Tian Z. Guided wave phased array beamforming and imaging in composite plates. *Ultrasonics* 2016;68:43–53.
- [12] Liu Z, Sun K, Song G, He C, Wu B. Damage localization in aluminum plate with compact rectangular phased piezoelectric transducer array. *Mech Syst Sig Process* 2016;70–71:625–36.
- [13] Xu C, Yang Z, Tian S, Chen X. Lamb wave inspection for composite laminates using a combined method of sparse reconstruction and delay-and-sum. *Compos Struct* 2019;223:110973.
- [14] Xu C-B, Yang Z-B, Zhai Z, Qiao B-J, Tian S-H, Chen X-F. A weighted sparse reconstruction-based ultrasonic guided wave anomaly imaging method for composite laminates. *Compos Struct* 2019;209:233–41.
- [15] Liu K, Ma S, Wu Z, Zheng Y, Qu X, Wang Y, et al. A novel probability-based diagnostic imaging with weight compensation for damage localization using guided waves. *Struct Health Monit: Int J* 2016;15(2):162–73.
- [16] Liu Y, Hong X, Zhang B. A novel velocity anisotropy probability imaging method using ultrasonic guided waves for composite plates. *Measurement* 2020;166: 108087.
- [17] Zhou C, Su Z, Cheng Li. Probability-based diagnostic imaging using hybrid features extracted from ultrasonic Lamb wave signals. *Smart Mater Struct* 2011;20(12): 125005.
- [18] Nokhbatolfoghai A, Navazi HM, Groves RM. Using the hybrid DAS-SR method for damage localization in composite plates. *Compos Struct* 2020;247:112420.
- [19] Sharif-Khadaei Z, Aliabadi MH. Assessment of delay-and-sum algorithms for damage detection in aluminium and composite plates. *Smart Mater Struct* 2014;23 (7):075007.
- [20] Shan S, Qiu J, Zhang C, Ji H, Cheng L. Multi-damage localization on large complex structures through an extended delay-and-sum based method. *Struct Health Monit* 2016;15(1):50–64.
- [21] Levine RM, Michaels JE. Model-based imaging of damage with Lamb waves via sparse reconstruction. *J Acoust Soc Am* 2013;133(3):1525–34.
- [22] Wang CH, Rose JT, Chang F-K. A synthetic time-reversal imaging method for structural health monitoring. *Smart Mater Struct* 2004;13(2):415–23.
- [23] Michaels JE. Detection, localization and characterization of damage in plates with an in situarray of spatially distributed ultrasonic sensors. *Smart Mater Struct* 2008; 17(3):035035.
- [24] Bekas DG, Mendias MM, Sharif Khodaei Z, Karachalias E, Alonso FJC, Aliabadi FMH. SHM of composite mono-stringer elements based on guided waves. *Key Eng Mater* 2019;827:464–9.
- [25] Grozdić DT, Jovičić ST, Subotić M. Whispered speech recognition using deep denoising autoencoder. *Eng Appl Artif Intell* 2017;59:15–22.
- [26] Saleh Ahmed A, El-Behaidy WH, Youssif AAA. Medical image denoising system based on stacked convolutional autoencoder for enhancing 2-dimensional gel electrophoresis noise reduction. *Biomed Signal Process Control* 2021;69:102842.
- [27] H L. On waves in an elastic plate. *Proc R Soc Lond A* 1917;93:114–28.
- [28] Nokhbatolfoghai A, Navazi HM, Groves RM. Use of delay and sum for sparse reconstruction improvement for structural health monitoring. *J Intell Mater Syst Struct* 2019;30(18–19):2919–31.
- [29] Xu W, Li X, Zhang J, Xue Z, Cao J. Ultrasonic signal enhancement for coarse grain materials by machine learning analysis. *Ultrasonics* 2021;117:106550.
- [30] Su C, Jiang M, Liang J, Tian A, Sun L, Zhang L, et al. Damage assessments of composite under the environment with strong noise based on synchrosqueezing wavelet transform and stack autoencoder algorithm. *Measurement* 2020;156: 107587.
- [31] Lin M, Chang F-K. The manufacture of composite structures with a built-in network of piezoceramics. *Compos Sci Technol* 2002;62(7–8):919–39.
- [32] Qing X, Beard S, Kumar A, Chan H, Ikegami R. Advances in the development of built-in diagnostic system for filament wound composite structures. *Compos Sci Technol* 2006;66(11–12):1694–702.
- [33] Rose JL. Ultrasonic guided waves in solid media: Science Press; 2019.